

Tunable large surface dielectrophoretic tweezer array: simulations and experimental validation

N.Ruyssen^{1,2}, B.Oliva³, Lylian Challier³, Vincent Noël³ and Benjamin Rotenberg^{2,4}

1. Delft University of Technology, Faculty of Civil Engineering and Geosciences, Environmental Fluid Mechanics, Box 5048, 2600 GA, Delft, The Netherlands.

2. Sorbonne Université, Physico-Chimie des Electrolytes et Nanosystèmes Interfaciaux, PHENIX, CNRS UMR 8234, Paris F-75005, France.

3. Université Paris Cité, Laboratoire ITODYS, CNRS UMR, Paris 7086, France.

4. Réseau sur le Stockage Electrochimique de l'Energie (RS2E), FR CNRS 3459, CNRS, Amiens 80039, France

Abstract

The ability to separate and isolate living microparticles such as phytoplankton is crucial for biological analysis, yet remains technically demanding [1]. Traditional microseparation and isolation methods often rely on physical membranes which can only separate particles by size. While effective in some contexts, these membranes introduce fabrication complexity, are prone to clogging and can induce unwanted mechanotransduction. In response to these limitations, we introduce a new membrane-less alternative based on dielectrophoresis (DEP) able to selectively separate and isolate one to two microparticles at specific controlled trapping sites. Our approach leverages recent advances in large-surfaces microfabrication, particularly High Precision Capillary Printing (HumminK), to construct complex electrode architectures rapidly and with high fidelity. Thanks to Finite Element (FE) simulations (COMSOL), we show that crossing the electrode arrays creates a field-induced grid of virtual pillars and field minima which functioning principle is close to that of optical tweezer arrays but at low frequency and compatible with large surfaces designs. This system exhibits two key modes of operation in negative DEP: selective particle trapping at precise stagnation sites and focusing along specific lines passing between the field-induced virtual pillars. We precisely identify the key parameter responsible for the switch between both modes that we have named “critical DEP mobility”. Using parametric analysis (COMSOL), we show that we can accurately control this critical DEP mobility by tuning the system geometry, the imposed voltage and flow rates. This tuning possibility is very important because it allows to tailor the device to a specific targeted microparticle and medium. Finally, we experimentally validate this concept by performing the selective capture of polystyrene particles by size with two different electrode geometry variations. This work is based on research we recently published in [2]. The present paper focuses on the modeling approach in COMSOL Multiphysics®, with an emphasis on simulation strategies and implementation.

Keywords: Dielectrophoresis, membrane-less, tweezer array, microparticle

Introduction

Efficient separation of colloidal particles, typically measuring between 1 and several tens of micrometers, plays a vital role in numerous sectors, including food and beverage processing, wastewater treatment, metal recovery, and biological sample analysis [2]. While micro-separation techniques have been successfully applied in many of these areas, some challenges remain. For example, selectively separating phytoplankton species from marine samples is especially challenging due to the large volumes involved and the wide diversity in particle size and morphology [2].

Traditional micro-separation methods using passive physical membranes, such as micropillar arrays or porous media, become less effective in this context. These systems suffer from high hydraulic resistance and membrane fouling, and they generally sort particles based on size only, making them partially adequate for mixtures containing particles with similar sizes but different shapes.

Several systems based on dielectrophoresis (DEP) reported in the literature have successfully separated microparticles by accumulating them on microfluidic channel walls, electrodes, or PDMS pillar arrays. However, to the author's knowledge, no DEP-based systems can arrange very small groups (one to two) of microparticles spatially like a selective large surface membrane-less DEP tweezer array. Designing such systems remains challenging, as it requires shaping the DEP force field across the channel using electrodes located at its boundaries.

Recent advances in electrode microfabrication techniques, such as High Precision Capillary Printing (Humink), enable the fabrication of thin electrode patterns over large surface areas. These developments open new possibilities for innovative electrode-based DEP system designs.

In this study, we introduce a novel concept for membrane-less DEP tweezing compatible with large-scale microfabrication techniques like High Precision Capillary Printing. This device enables selective separation based on DEP mobility, without requiring contact between particles and channel walls or electrodes, minimizing both mechanical stress and Joule heating.

This work is based on research we recently published in [2]. We particularly focus the present

paper focuses on the modeling approach and its implementation in COMSOL Multiphysics®.

Theory & Experimental Set Up

Microparticle dielectrophoresis

DEP is the motion of polarizable particles in a medium due to the presence of an electric field gradient. In the dipole-approximation and assuming a spherical particle shape, the (time-averaged) net DEP force experienced by such particles is:

$$\mathbf{F}_d = 2\pi\epsilon_m R^3 \mathcal{R}(K^*) \boldsymbol{\xi}$$

where ϵ_m is the medium absolute permittivity, R the particle radius, $\mathcal{R}(K^*)$ the real part of the Clausius-Mossotti factor K^* and $\boldsymbol{\xi} = \nabla E^2$ the Mean-square (MS) electric field gradient. When $\mathcal{R}(K^*)$ is negative (negative DEP), particles are attracted towards the E^2 minima. The Clausius-Mossotti factor K^* represents the particle polarizability in the given medium and is defined by:

$$K^* = \frac{\epsilon_p^* - \epsilon_m^*}{\epsilon_p^* + 2\epsilon_m^*}$$

Where $\epsilon_p^* = \epsilon_p - i\frac{\sigma_p}{\omega}$ and $\epsilon_m^* = \epsilon_m - i\frac{\sigma_m}{\omega}$ are the particle and medium complex permittivities respectively with $\omega = 2\pi f$ the voltage pulsation, f the voltage frequency and σ_p and σ_m the particle and medium electric conductivities respectively. In addition, particles in a fluid flow experience a fluid hydrodynamic drag force given the Stokes law:

$$\mathbf{F}_h = 6\pi R\mu(\mathbf{u} - \mathbf{v})$$

Where μ is the (fluid) medium dynamic viscosity, \mathbf{u} the medium velocity and \mathbf{v} the particle velocity. The trapping of particles is possible when the hydrodynamic force \mathbf{F}_h is balanced by the DEP force \mathbf{F}_d .

Device geometry

Figure 1(a) introduces the proposed device for DEP tweezing. It is made of two pairs of interdigitated electrode arrays: one at the top (blue and yellow electrodes Figure 1(a) and (b)) and one at the bottom (red and green electrodes Figure 1(a) and (b)) of a microfluidic channel. The electrode arrays are inclined with respect to the flow direction with angles α and $-\alpha$ respectively. Therefore, the top and bottom electrode arrays appear as “crossed” in top view (pink dashed box Figure 1(a)). The DEP tweezer array is in this specific region and its

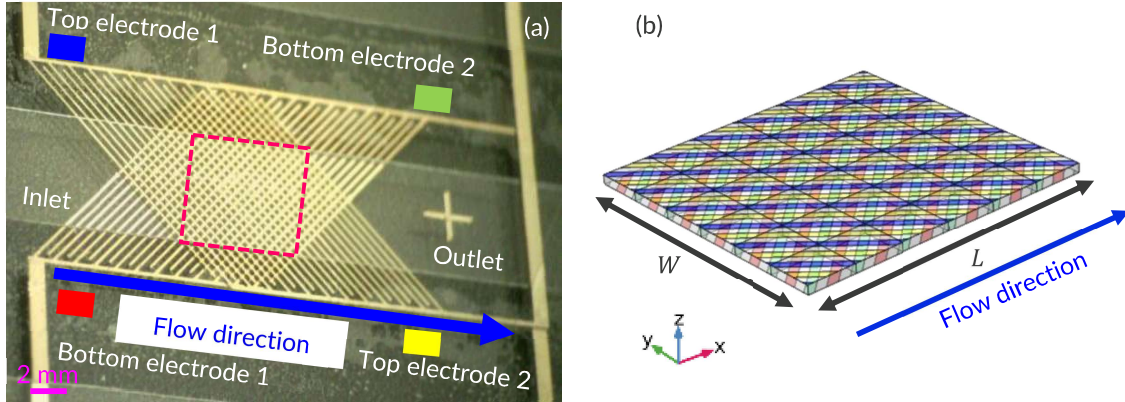


Figure 1 (a) The device fabricated geometry by High Precision Capillary Printing (Humminck). (b) Periodic geometry of the electrode arrays used for modelling corresponding to the pink boxed region on panel (a), the colors of the electrodes match the colors indicated on panel (a), for sake the of clarity. Reproduced from [2]. © IOP Publishing.

periodic geometry used for simulations is shown Figure 1 (b)

Numerical Simulations

Electroquasistatic problem

To predict particle behavior, the DEP field factor $\xi = \nabla E^2$ must be determined. We apply electric field in the low frequency range (10 MHz), so that the electromagnetic propagation delays are negligible with respect to time variations of the electric field. Therefore, in the frequency domain, the charge conservation equation reduces to the Laplace equation of the root-mean-square (RMS) electric potential ϕ :

$$\nabla^2 \phi = 0$$

As boundary conditions, we prescribe the RMS electric potential ϕ to the applied RMS potential V on the positively charged electrodes (yellow electrodes Figure 2(a)) and we prescribe null RMS potential ϕ on the grounded electrodes (blue electrodes Figure 2(a)). On the channel walls boundaries (in grey between the electrodes Figure 2(a)), we apply a perfect insulator boundary condition: $-\mathbf{E} \cdot \mathbf{n} = \frac{\partial \phi}{\partial n} = 0$ where \mathbf{n} is the outward unitary normal vector to the boundary of Ω_p . Finally, we consider periodic boundary conditions on the lateral opposite faces of the frontiers of Ω_p . This boundary problem is translated into the following weak-form equation and is implemented into COMSOL (Weak form PDE module):

$$\int_{\Omega_p} -\nabla \phi \cdot \nabla \psi \, d\Omega_p + \oint_{\partial \Omega_p} \frac{\partial \phi}{\partial n} \psi \, d\partial \Omega_p$$

Where ψ is the test function and $\partial \Omega_p$ the boundary of Ω_p . Note that the AC/DC module or the Laplace equation module can also solve such equation. The latter weak form equation is discretized in space using cubic Lagrange polynomials and the resulting linear system is numerically solved using the COMSOL Multifrontal Massively Parallel Sparse (MUMPS) solver.

Microfluidic problem

The fluid mass transport equation with the flow incompressibility condition reduces to:

$$\nabla \cdot \mathbf{u} = 0$$

Where \mathbf{u} is the fluid medium velocity field. In addition, the linear momentum balance equation at low Reynolds number, low particle concentration, for a Newtonian fluid and in stationary regime reduces to the Stokes equation:

$$-\nabla p + \mu \nabla^2 \mathbf{u} = \mathbf{0}$$

Where p is the fluid pressure field assumed uniform on the channel's inlet and outlet. On the channel walls, we consider a no-slip boundary condition. The two latter equations with their respective boundary conditions can be numerically solved (e.g. using the laminar flow or microfluidics modules), but for this simple channel geometry, the analytical solution of the fluid velocity can be found using y and z series expansions. Since the channel depth H is low with respect to the channel

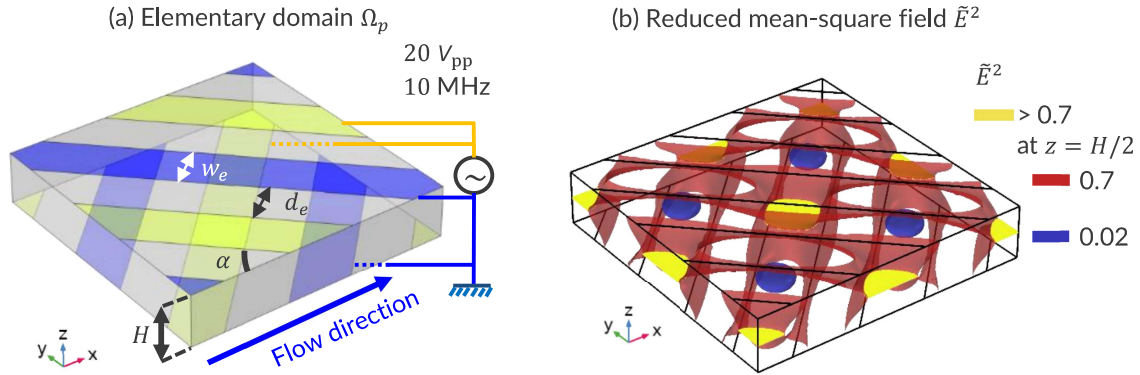


Figure 2. (a). Parameterized geometry of the model elementary domain (period, Ω_p), w_e is the electrode width, d_e the electrode spacing, α the electrode/flow angle and H the microfluidic channel depth. The blue top and bottom electrodes are grounded whilst a sinusoidal electric potential is applied on the yellow top and bottom electrodes. (b) Reduced mean-square electric field $\tilde{E} = E^2(H/V)^2$ topology depicted by three iso-surface plots. Reproduced from [2]. © IOP Publishing.

width W , the fluid velocity norm u is well approximated by the Poiseuille flow solution:

$$u(z) \approx U \left[1 - 4 \left(\frac{z'}{H} \right)^2 \right]$$

Where U is the maximal fluid velocity located in the channel's mid-plane (at $z = H/2$) and with $z' = z - H/2$.

Microparticles dynamics

We neglect particles inertia. The knowledge of ϕ and \mathbf{u} , allows the calculation of the particle velocity:

$$\frac{\partial \mathbf{r}}{\partial t} = \mathbf{u} + m_d \boldsymbol{\xi}$$

Where \mathbf{r} is the particle position and $m_d = R^2 \epsilon_m \mathcal{R}(K^*) / 3\mu$ is the particle DEP mobility. Since we ignore the local flow and electric field perturbations due to the presence of particles (one-way coupling). The latter equation can be simply solved in time using an explicit Runge-Kutta scheme in COMSOL with the particle tracing module or with a streamline plot (in stationary regime) using the particle velocity: $\mathbf{u} + m_d \boldsymbol{\xi}$.

Results

Electric field pillar and trap array

The reduced MS electric field $\tilde{E}^2 = \left(\frac{EH}{V} \right)^2$ topology is shown Figure 2(b) in iso-surface representation. The particle repulsive zones in negative DEP (when $\mathcal{R}(K^*) < 0$) are the high field regions (red and yellow iso-surfaces) which exhibit a vertical pillar array shape (in the Oz direction with a yellow cross section in the channel's mid-plane Figure 2(b)).

These high field zones are located where two electrodes of opposite polarities are crossing in top view (Figure 2(a), when a yellow electrode crosses a blue electrode in top view). Conversely, the particle attractive zones in negative DEP are the low field regions (blue iso-surface Figure 2(b)) which display an ellipsoid-like array shape. These zones are located where electrodes of same polarity are crossing in top view (Figure 2(a), when electrodes of same color cross in top view) and may be able to trap particles if the DEP force field is important enough.

Focusing and capture of particles

Figure 3 shows the calculated particle trajectories initially regularly distributed on the channel's cross section (in green) for an applied RMS voltage on the electrodes of $V = 7.07$ V (20 V peak-to-peak) and frequency $f = 10$ MHz. We note that both $5 \mu\text{m}$ and $25 \mu\text{m}$ PS beads vertically focus in the channel mid plane (at $z = \frac{H}{2}$ Figure 3(a) and (b)).

We see Figure 3(c) that $5 \mu\text{m}$ particles laterally focus between the field virtual pillars along the lines linking the field minima in the flow direction that we call "focusing lines" in the following. The $25 \mu\text{m}$ particles also laterally focus along the latter and converge at stable stagnation points (Figure 3(b) and (d)). The existence condition of stagnation points corresponds to the following equation:

$$\mathbf{u} + m_d \boldsymbol{\xi} = \mathbf{0}$$

The vertical and lateral projections of this relation imply that particles can be captured only in the channel mid plane and along the focusing lines respectively (in negative DEP). The projection of

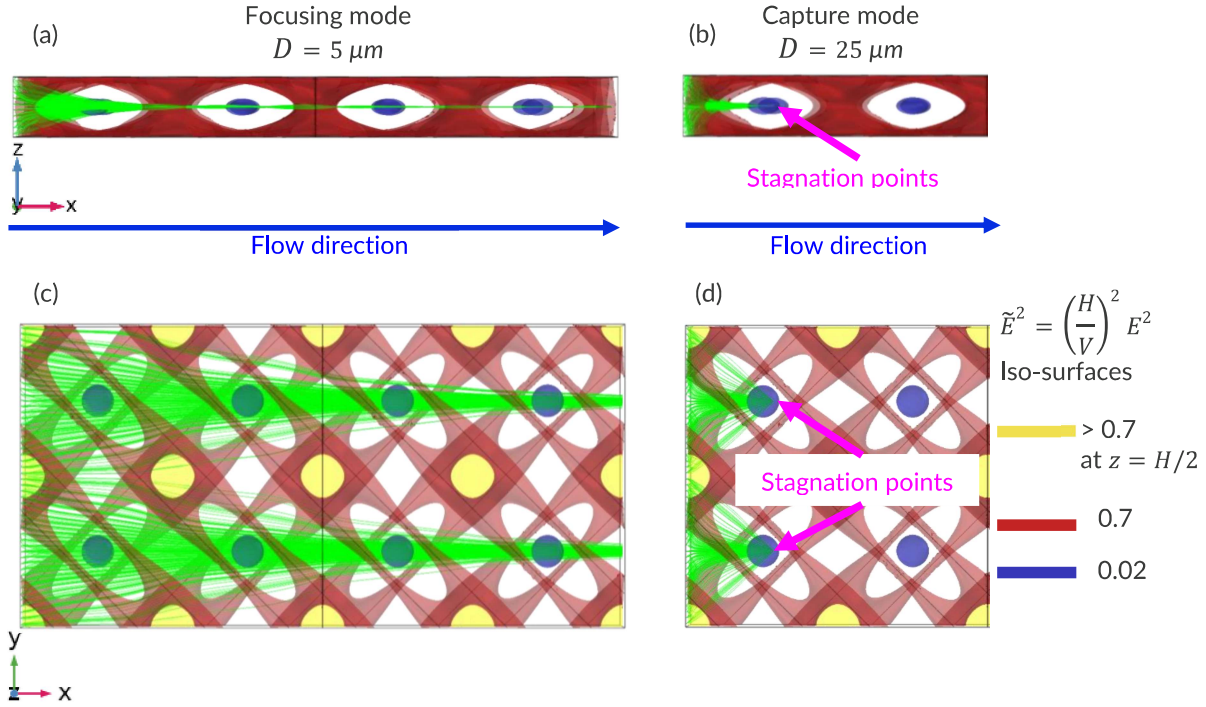


Figure 3. Independent particles trajectories (green) in side view for $D=5 \mu\text{m}$ (a) and $D=25 \mu\text{m}$ (b) diameter PS beads and a frequency $f = 10 \text{ MHz}$, the particle trajectories rapidly focus in the channel mid-plane and a stagnation point appears in the channel mid-plane. Particles trajectories in top view laterally focusing between the field virtual pillars for $5 \mu\text{m}$ (c) and $25 \mu\text{m}$ (d) PS bead. Stagnation points appear for the $25 \mu\text{m}$ particle trajectories near the field minima (blue iso-surfaces). Reproduced from [2]. © IOP Publishing.

the stagnation condition in the flow direction and in the channel mid plane reads:

$$U + m_d \xi_x = 0$$

where $\xi_x = \frac{\partial E^2}{\partial x}$ is the DEP field factor component along the flow direction. In other words, particles with DEP mobility m_d can be stopped if the streamwise component of the DEP field factor ξ_x at the focusing lines is important enough so that the latter stagnation condition is verified. Therefore, it exists a certain particle critical mobility m_d^c which allows to anticipate whether a particle can be trapped or not in the low field regions. This critical mobility is related to the maximum value of ξ_x along the focusing lines ξ_{max} and is defined by:

$$m_d^c = -\frac{U}{\xi_{max}} = -\frac{UH^3}{V^2 \xi_{max}}$$

Where $\tilde{\xi}_{max} = \frac{H^3}{V^2} \xi_{max}$ is the reduced DEP field factor. Since the maximal fluid velocity U , the applied RMS voltage V and the channel depth H can be experimentally controlled, it is of interest to predict the evolution of the reduced DEP field

factor $\tilde{\xi}_{max}$ with respect to the device geometry. To do so, we performed parametric studies for the device geometric parameters.

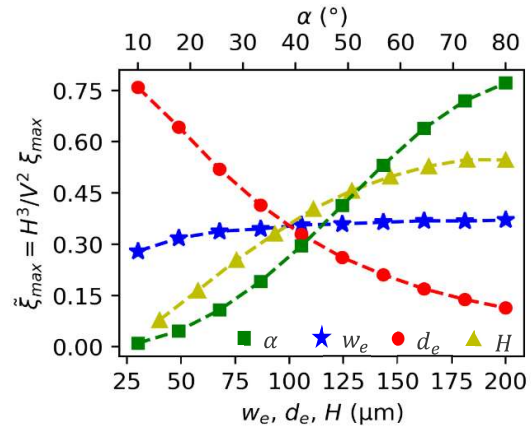


Figure 4. Single parametric study results on the reduced maximal DEP field factor along the focusing lines $\tilde{\xi}_{max}$. When parameters are fixed, their values are $w_e = d_e = H = 100 \mu\text{m}$ and $\alpha = 45^\circ$. Each point corresponds to a simulation. Reproduced from [2]. © IOP Publishing.

Controlling the capture condition of particles

Figure 4 displays the influence of each geometric parameter on the reduced maximum DEP field factor along the focusing lines ξ_{max} . We see the influence of the electrode width w_e is very low when $w_e \geq 0.8H$ (blue stars curve, Figure 4(a)), in this case, the maximum MS electric field in the virtual pillar cross section is $E^2 \approx \left(\frac{V}{H}\right)^2$ which corresponds to the value of the MS electric field in an infinite planar capacitor. Therefore, there is no interest in choosing an electrode width w_e superior to $0.8H$ and we will keep $w_e = 0.8H$. Even though the electrode-flow angle α has a significant influence on ξ_{max} (sinus-like, green square curve Figure 4), choosing $\alpha = 45^\circ$ maximizes the trap

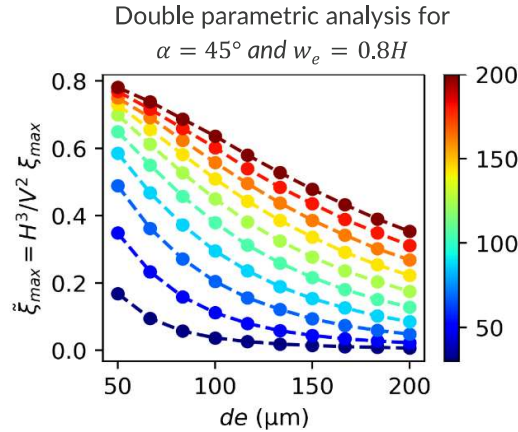


Figure 5. Double parametric (d_e, H) study results on the reduced maximal DEP field factor along the focusing lines ξ_{max} . The electrode-flow angle α is fixed to 45° and the electrode width w_e proportionally varies with H such that $w_e = 0.8H$. Each point corresponds to a simulation. Reproduced from [2]. © IOP Publishing.

surface density. Thereby, we keep $\alpha = 45^\circ$ in the following. Finally, both the electrode spacing d_e and the channel depth H have important influences on ξ_{max} , their combined influences should be tested in a double parametric study. The results of such study are visible Figure 5: this curve family plot shows 100 possibilities for (d_e, H) values to tune ξ_{max} and thus the critical mobility m_d^c . The latter parameter value should be adapted to the targeted microparticle.

Application and experimental validation

By replacing the DEP mobility expression $m_d = R^2 \epsilon_m \mathcal{R}(K^*) / 3\mu$ in the critical mobility m_d^c expression, we can express the corresponding critical diameter:

$$D_p^c = \frac{H}{V} \sqrt{\frac{18 \mu}{\epsilon_m |\mathcal{R}(K^*)|}} \sqrt{\frac{Q}{W \xi_{max}}}$$

Where $Q = \frac{2}{3} UWH$ is the fluid flow rate in the channel. This formula, combined with the simulation results Figure 5 relates the critical particle size to the experimental parameters. To validate the presented membrane-less DEP tweezer array concept, we use the latter formula for two easily fabricable geometric variations of the device: $d_e = 100 \mu\text{m}$, $H = 70 \mu\text{m}$ to observe the focusing mode of $25 \mu\text{m}$ PS-beads and $d_e = 50 \mu\text{m}$, $H = 50 \mu\text{m}$ to observe the capture mode of the same particles.

Figure 6 shows the particles in the experimental device made to observe $25 \mu\text{m}$ particle focusing without capture. We note that $25 \mu\text{m}$ particles align in the flow direction and continue moving along specific lines where electrodes are crossing (blue dashed lines Figure 6). These lines are the focusing lines identified in the simulation results. Moreover, we note the absence of particles between every pair of focusing lines where electrodes are also crossing in top view (red lines Figure 6) These lines are the virtual pillar rows identified in the simulation results. For experimental movies, see the supplementary materials to [2].

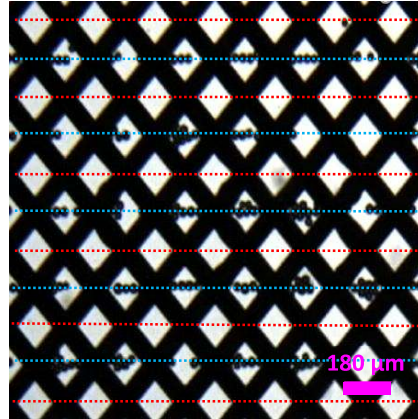


Figure 6. Microscopy observation of the focusing mode of $25 \mu\text{m}$ PS-beads. Reproduced from [2]. © IOP Publishing.

Figure 7 displays the particles in the experimental device tuned to observe $25 \mu\text{m}$ particle capture. We note the capture of one to two $25 \mu\text{m}$ particles (green circles Figure 7) along the focusing lines (blue dashed lines Figure 7) slightly downstream to the electrode “intersections” in top view. Indeed, the DEP field factor ξ is null at the exact “intersections” of the electrodes in top view and this equilibrium position corresponds to a no-flow configuration. In presence of a fluid flow, the

equilibrium position should be a little downstream to the electrode “intersections” where the DEP force field F_d is not null and important enough to balance the hydrodynamic drag force F_h . For more explanation about the exact location of the capture position and experimental movies, see [2]. Finally, 5 μm PS beads of diameter below the critical diameter, theoretically too small to be captured, were also introduced into the device. We can see these smaller particles following the fluid flow while being slightly repelled by the virtual pillars Figure 7 (red circles), which confirms the system ability to selectively trap targeted particles by size.

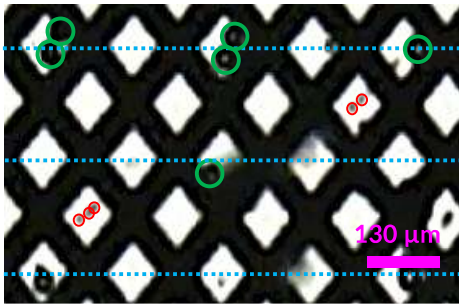


Figure 7. Microscopy observation of the capture mode of 25 μm PS beads (green circles) while 5 μm PS beads are not captured (red circles). Reproduced with permission from [2]. © IOP Publishing.

Conclusions and perspectives

We developed a numerical model that allowed the design of a new membrane-less selective dielectrophoretic tweezer array compatible with large surface electrode microfabrication processes. Thanks to the simulations, we accurately identified the microparticles capture condition and the concept was experimentally validated. Finally, since the user can easily control the system critical mobility, the same system could be used to determine unknown particle DEP mobility [2]. This paper focused on the modelling aspects of the study. For more information, see [2].

References

- [1] Challier, L., Lemarchand, J., Deanno, C., Jauzein, C., Mattana, G., Mériquet, G., ... & Noël, V. (2021). Printed Dielectrophoretic Electrode-Based Continuous Flow Microfluidic Systems for Particles 3D-Trapping. *Particle & Particle Systems Characterization*, 38(2), 2000235..
- [2] Ruysen, N., Oliva, B., Challier, L., Noël, V., & Rotenberg, B. (2025). Tunable membrane-

less dielectrophoretic microseparation by crossing interdigitated electrodes. *Journal of Physics D: Applied Physics*, 58(18), 185309.

Acknowledgements

This project received funding from the ANR (Grant Number ANR-21-CE29-0021-02) and from the European Research Council under the European Union’s Horizon 2020 research and innovation program (Grant Agreement No. 863473). The authors thank the PRINTEC platform from ITODYS laboratory for providing access to advanced printing and characterization instruments, as well as for their technical support.